

Combinatorial substrate epitaxy: A high-throughput method for determining phase and orientation relationships and its application to BiFeO₃/TiO₂ heterostructures

Yiling Zhang, Andrew M. Schultz, Li Li, Harry Chien, Paul A. Salvador, Gregory S. Rohrer*

Department of Materials Science and Engineering, Carnegie Mellon University, Pittsburgh, PA 15213, USA

Received 6 May 2012; received in revised form 26 July 2012; accepted 28 July 2012

Available online 18 September 2012

Abstract

A new technique, combinatorial substrate epitaxy, has been used to study the polymorphic stability and orientation relationships (ORs) for TiO₂ thin films grown by pulsed laser deposition on polycrystalline BiFeO₃ at 600 °C. Electron backscatter diffraction data from 150 substrate/film pairs were analyzed to determine that anatase (A) grew with the OR (112)_A || (111)_{BFO} and [1 $\bar{1}$ 0]_A || [1 $\bar{1}$ 0]_{BFO} on BiFeO₃ (BFO) substrates oriented within 35° of [100]. Rutile (R) was found on all other substrate orientations with (100)_R || (111)_{BFO}. The in-plane orientation was primarily [001]_R || [1 $\bar{1}$ 0]_{BFO}, but some films near the anatase/rutile phase boundary were rotated by 30° so that [001]_R || [$\bar{1}$ 2 $\bar{1}$]_{BFO}. Because these substrate film pairs have high-index interface planes, conventional epitaxy arguments based on two-dimensional lattice mismatch in low-index planes are considered to be limiting cases of a more general model involving the three-dimensional alignment of closest packed planes and directions, regardless of the interface plane.
© 2012 Acta Materialia Inc. Published by Elsevier Ltd. All rights reserved.

Keywords: Epitaxy; Crystal growth; EBSD; Interfaces; Orientation relationships

1. Introduction

TiO₂ films on BaTiO₃ substrates have been shown to exhibit novel photochemical activity, including spatially localized reactivity governed by the underlying ferroelectric domain structure [1–3]. More recently, it has been demonstrated that when TiO₂ is supported on ferroelectric BiFeO₃, it demonstrates a similar spatially selective reactivity, but is also photochemically active in visible light (unlike bulk TiO₂ or TiO₂ supported on BaTiO₃) [4]. Titania films crystallize in both the rutile and anatase structures when deposited on perovskite-structured BiFeO₃. Because the photochemical reactivity of titania is known to depend on both its phase [5] and orientation [6–8], it is

of interest to determine the orientation relationships (ORs) for BiFeO₃/TiO₂ heterostructures.

Currently, little is known about the crystallization preferences of films on high-index surfaces. Epitaxy in thin films is usually ascribed to preferred lattice matching at low-index two-dimensional interfaces [9]; the extension of such theories to high-index surfaces is difficult. To better understand the nature of crystallization of films on general surfaces, it is necessary to observe growth over the entire range of possible surface orientations. The conventional approach of growing films on large-area, low-index, single-crystal substrates is not practical for a comprehensive study of growth on high-index surfaces.

This paper has two purposes. The first is to describe a new high-throughput technique we refer to as “combinatorial substrate epitaxy” (CSE) to determine phase relationships and ORs between a substrate and deposited film for all possible orientations. In the CSE approach, films are

* Corresponding author. Tel.: +1 412 268 2696; fax: +1 412 268 7596.
E-mail address: gr20@andrew.cmu.edu (G.S. Rohrer).

deposited on hundreds of substrates with different, known orientations in a single experiment and then characterized by electron backscatter diffraction (EBSD). The second purpose is to describe the specific phase and ORs in the BiFeO₃/TiO₂ system and show that epitaxy in this system is driven by the alignment of close-packed planes and directions in three dimensions.

Although BiFeO₃ is trigonal, the distortion from cubic is small ($\alpha = 89.3^\circ$) and it can be considered as a pseudocubic perovskite ($a = 3.96 \text{ \AA}$); this simplification will be made throughout this paper [10]. While the ORs in BiFeO₃/TiO₂ heterostructures have not been reported before, there have been a number of studies reporting the growth of TiO₂ on LaAlO₃ ($a = 3.790 \text{ \AA}$ [11]), SrTiO₃ (3.905 \AA [12]) and BaTiO₃ (3.9920 \AA [12]) [13–27]. While the experiments span a range of materials, temperatures and growth techniques, there are a few common features. The first is that for growth on (001) oriented substrates, the most common OR is $(001)_A \parallel (001)_P$ and $[100]_A \parallel [100]_P$, where A denotes anatase and P denotes perovskite [13–16,19,20,23,25–27]. The second common feature is that on perovskite (111), rutile grows in the (100) orientation [13,21,22,27]. These observations have been rationalized using lattice-matching arguments; the relevant lattice parameters are listed in Table 1 [10–12,28,29].

With the exception of the paper by Burbure et al. [13], all of the previous studies used single-crystal substrates with low-index orientations. Burbure et al. [13] grew TiO₂ films on a polycrystalline BaTiO₃ substrate and used EBSD in a scanning electron microscope to determine the orientations of the substrate and film grains. In the present paper, we present a technique based on the same experimental concept, but with an improved analysis method that makes it easier to determine the ORs. Through the analysis of 150 BiFeO₃ substrate/TiO₂ film pairs, the range of substrate orientations that stabilize epitaxial anatase and rutile have been determined as well as the ORs for each of these phases. In the vast majority of the cases, epitaxial growth occurs on high-index planes and aligns the close-packed planes and directions that are common to each phase.

2. Experimental methods

A polycrystalline BiFeO₃ substrate was synthesized from Bi₂O₃ (Alfa Aesar 99.99%) and Fe₂O₃ (99.945%) powders [30]. Equimolar amounts of both powders were mixed and ball milled in ethanol for 24 h, and dried at 85 °C. The mixture was calcined in air at 700 °C for 3 h to form BiFeO₃ powder, as verified by X-ray diffraction.

The BiFeO₃ powder was ground, ball milled in ethanol for 24 h, dried and compressed uniaxially at 105 MPa to form a pellet $\sim 1 \text{ cm}$ in diameter and 3 mm thick. The BiFeO₃ pellet was sintered at 850 °C for 3 h. One side of the pellet was ground with an aqueous Al₂O₃ suspension (3 μm , Logitech) and polished with a SiO₂ colloidal suspension (0.02 μm , MasterMet 2, Buehler) using a Logitech autopolisher. The polished pellets were then annealed at 600 °C for 3 h in air to heal polishing damage.

After preparing the BiFeO₃ substrate, the orientation of each grain within an area of approximately $1.2 \times 1.2 \text{ mm}^2$ on the surface was determined using EBSD in a Quanta 200 scanning electron microscope (FEI, Hillsboro, OR) [31]. The substrate surface was tilted at 70° with respect to the beam direction in high vacuum (10^{-5} torr). The beam energy was set at 25 keV, the spot size was 5.5 and the working distance was 15 mm. The Kikuchi patterns were indexed using TSL orientation imaging microscopy data collection and analysis software (EDAX, Mahwah, NJ). The orientation data was processed as described previously [30].

After the substrate orientations had been measured, a TiO₂ film was grown on the BiFeO₃ substrate using pulsed laser deposition (PLD) [32]. The TiO₂ target was synthesized by compressing TiO₂ powder in a die to form a disc $\sim 2.5 \text{ cm}$ in diameter and $\sim 1.4 \text{ mm}$ thick, and then sintering it at 1400 °C for 12 h. Before depositing the TiO₂ film, the chamber was pumped down to reach a base pressure of 10^{-5} torr with the substrate heated to 120 °C. Oxygen was then introduced to the chamber and a partial pressure of 5 mTorr was maintained. The substrate was then heated to 600 °C at a rate of 25 °C min⁻¹. A KrF ($\lambda = 248 \text{ nm}$) laser with an energy density of 2 J cm⁻² was pulsed at 3 Hz for 10 min to clean the target. During the deposition, the target-to-substrate distance was maintained at approximately 6 cm. The deposited film was estimated to be 100 nm thick, based on the number of laser pulses and the measured deposition rate, as reported previously [4]. After the deposition, the substrate was cooled to room temperature at a rate of 25 °C min⁻¹ in an atmosphere of 5 torr stagnant oxygen.

The TiO₂ film on the BiFeO₃ substrate was characterized by EBSD using a procedure that is similar to that used for the BiFeO₃ substrate. One source of error in the determination of the OR stems from alignment of the sample during the orientation mapping. Because the sample is removed from the microscope after the substrate mapping, and then returned for mapping the film, a small misalignment will result in a constant average misorientation between the substrate and film data that will be superimposed on the typical uncertainty associated with the orientation measurement.

The procedure for finding the ORs begins by manually matching substrate grains with film grains by visual inspection of orientation maps, such as those shown in Fig. 1. For example, based on the similar position and shape, one can deduce that the grains marked by the same symbols (A–D) on the substrate (Fig. 1a) and in the film (Fig. 1b) correspond to pairs. This makes it possible to create a list of matched pairs, in which the unique “grain

Table 1
Crystallographic parameters for BiFeO₃ and TiO₂ [10–12].

Phase	Space group	Lattice parameter
BiFeO ₃	<i>R3c</i>	$a = 3.962 \text{ \AA}$, $\alpha = 89^\circ 31'$
Anatase TiO ₂	<i>I4₁/amd</i>	$a = 3.785 \text{ \AA}$, $c = 9.514 \text{ \AA}$
Rutile TiO ₂	<i>P4₂/mmm</i>	$a = 4.594 \text{ \AA}$, $c = 2.958 \text{ \AA}$

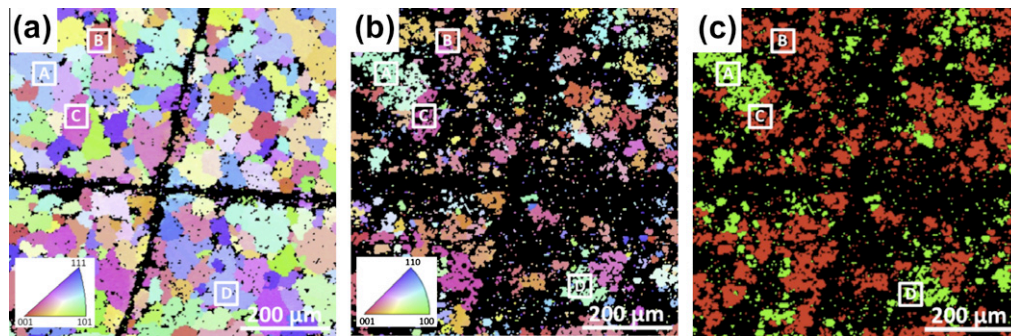


Fig. 1. (a) An orientation map of the BiFeO_3 substrate. The colors show the orientations of the grains with respect to the surface normal, according to the key in the inset. (b) An orientation map of the TiO_2 film, in the same area as (a). The surface normal orientations of anatase and rutile are shown by the color key in the inset. The grains in (a and b) marked with the same symbols (A–D) are substrate/film pairs. (c) A phase map of the TiO_2 film grown on BiFeO_3 substrate, in the same area as (b). Red indicates anatase and green indicates rutile. In all of the maps, black indicates areas with a confidence index less than 0.1. (For interpretation of the references to color in this figure legend, the reader is referred to the web version of this article.)

identification numbers” assigned arbitrarily by the TSL software are used to associate the substrate/film pairs. For this study, 150 substrate grain pairs were identified.

The remainder of the analysis is automated and based on the list of matched grain identification numbers. The orientation maps can be exported from the TSL software as text files that list the coordinates, orientation (in the form of Euler angles), phase and grain identification number for every point in the map. A program developed in our lab (*get_pairs*) searches these files for grain identification numbers in the pre-established list of matched pairs and records the Euler angles for the corresponding substrate and film grains. Both the raw data and the software (*CSE_software_v1.0*) for all operations are provided at a URL provided in the [Supplemental materials](#).

A second program (*ORs*) allows the ORs to be determined in the following way. The user selects a trial direction in the crystal reference frame of the substrate and another in the crystal reference frame of the film. For each substrate/film pair, these directions are transformed to the laboratory reference frame. The angle between these directions is then computed for each pair. In the calculation of the angle between the directions, it is important to recognize the crystal symmetry in each phase. In the calculation, the angles between all possible pairs of crystallographically indistinguishable directions are computed and the minimum angle is selected. As long as the film is epitaxial on the substrate, then the minimum angle between the two reference directions is constant in all of the substrate/film pairs. It is relatively simple to find the directions with the minimum misalignment, and this specifies one component of the OR. The process is repeated for directions perpendicular to the aligned axes to find the second component of the OR. An example of this procedure will be illustrated in Section 3.

3. Results

A representative portion of the orientation and phase data is shown in Fig. 1. The black areas are regions where

there was low confidence in the indexing, usually because there was a pore or inclusion of a second phase. This distribution of colors across the field of view indicates that there is no preferred orientation.

Only about 70% of the diffraction patterns are reliably indexed when the film orientations are indexed automatically, compared to more than 95% in the substrate. This is in part because the EBSD patterns from the film are of poorer quality than the substrate. Fig. 2 shows examples of EBSD patterns from the substrate and the film for comparison. Note that while the patterns from the film are more diffuse, bands can be identified and orientations can be assigned with reasonable confidence. Strain or defects in the epitaxial layer are likely factors that contribute to the reduced quality of the patterns from the film, but this has not been studied in any detail. It is also possible that orientations cannot be assigned because of the overlap of multiple patterns from two or more grains. If a single substrate grain supports a non-epitaxial, polycrystalline film, and the grain size of the film is less than or equal to the resolution (approximately 20 nm in an ideal sample [33] and probably lower here), then it will not be possible to assign reliable orientations to patterns from these areas. Even if a few points in such a region are reliably indexed, contiguous areas with a consistent orientation are needed to make a reliable correlation to a supporting substrate grain.

The 150 pairs of substrate/film orientations are shown in Fig. 3. There is a clear separation between the BiFeO_3 orientations that support the growth of anatase and those that support the growth of rutile. There is a band in which the measurements overlap, but considering that the typical orientation resolution in EBSD is $\pm 2^\circ$ [33], this is not unexpected. Grains orientated within 35° of [001] support anatase growth, while those closer to [101] and [111] support rutile growth. Note that there is an empty region near [111]. The data from the films on grains with these orientations was not reliably and consistently indexed by the automatic procedure. A manual inspection of the diffraction patterns from such grains indicated that multiple film orientations could be found on a single substrate grain.

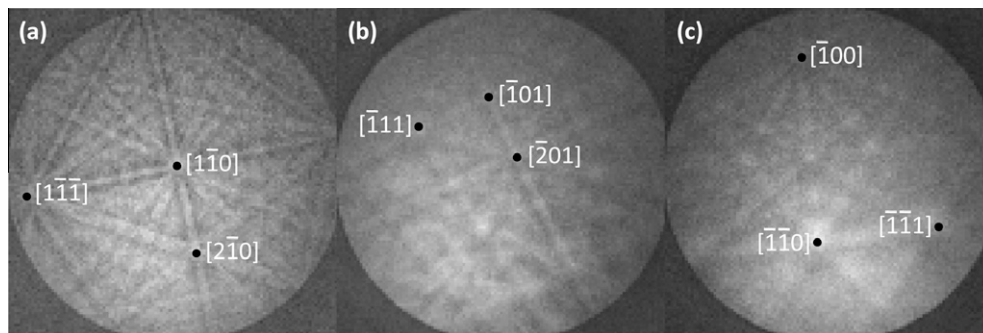


Fig. 2. Sample EBSD patterns for (a) a BiFeO₃ grain in the substrate ($\phi_1 = 189^\circ$, $\Phi = 84^\circ$, $\phi_2 = 184^\circ$), (b) an anatase TiO₂ grain ($\phi_1 = 48^\circ$, $\Phi = 15^\circ$, $\phi_2 = 155^\circ$) and (c) a rutile TiO₂ grain ($\phi_1 = 180^\circ$, $\Phi = 82^\circ$, $\phi_2 = 290^\circ$) in the film.

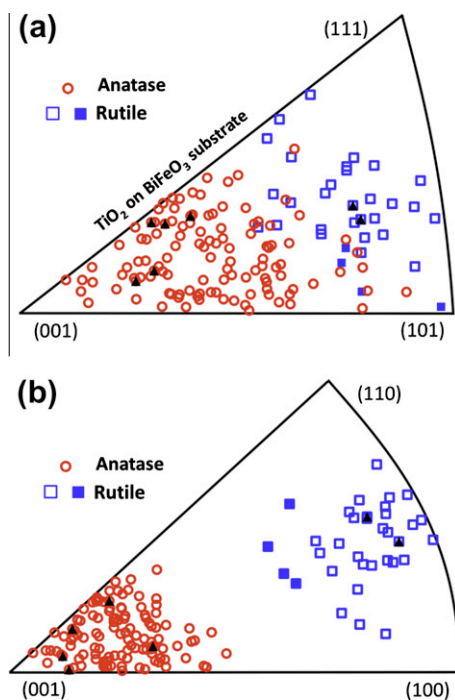


Fig. 3. (a) Orientations of BiFeO₃ grains that supported epitaxial TiO₂ growth in the standard stereographic triangle for cubic crystals. Red circles mark orientations that supported anatase and blue squares mark those that supported rutile. (b) Orientations of anatase/rutile TiO₂ grains in the standard stereographic triangle for tetragonal crystals. The seven points marked by the black triangles had ORs that were inconsistent with the other 143 points. (For interpretation of the references to color in this figure legend, the reader is referred to the web version of this article.)

When regions were identified with non-overlapping patterns, the film could always be indexed as rutile, but there was not a consistent OR. Therefore, it was concluded that BiFeO₃ grains near [111] support polycrystalline rutile.

The orientations of all of the indexed films are illustrated in Fig. 3b. These data provide some information about the ORs. The anatase that grows on BiFeO₃ in the vicinity of [001] is also clustered near the anatase [001] orientation. The rutile that grows on other orientations of BiFeO₃ has orientations that are nearly perpendicular to [001].

To determine the ORs, we begin by comparing the alignment of the closest-packed planes. Both the perovskite structure and the anatase structure can be considered as consisting of cubic close-packed arrangements of oxygen ions. In perovskite, the closest-packed planes are (111) and the analogous plane in anatase is (112). The angle between these two planes for the 115 substrate/anatase pairs is shown in Fig. 4a, where the horizontal axis is simply the order in which the data were recorded. The average misorientation (standard deviation) for the majority of the pairs is 2.6° (1.2°). The same calculation was repeated for the perpendicular $[1\bar{1}0]$ axes. In this case, 110 of the substrate/crystal pairs have $[1\bar{1}0]$ axes misoriented by an average angle (standard deviation) of 3.2° (1.8°). Therefore, based on 96% of the observations, we assign the OR to be $(112)_A \parallel (111)_{BFO}$ and $[1\bar{1}0]_A \parallel [1\bar{1}0]_{BFO}$. While the observed average misorientations are not exactly zero, it is reasonable that deviations of a few degrees would result from a combination of experimental uncertainty in the orientation measurements and misalignment of the sample during the two measurements.

Note that there are some obvious outliers in Fig. 4. These points are marked by black triangles in Fig. 3. All five of these points could be described (with an average misorientation of 8°) to have an OR of $(100)_A \parallel (210)_{BFO}$. This may be a secondary OR that is occasionally stabilized during growth, but was not investigated further.

The process was repeated for the 35 observed BiFeO₃/rutile pairs. The results, shown in Fig. 5, indicate two primary ORs. First, the angles between $[111]$ in BiFeO₃ and $[100]$ in rutile are shown in Fig. 5a. The average of these angles is 1.3° and there are two significant outliers. Next, looking at perpendicular axes, we find that nearly all of the $[110]$ axes in BiFeO₃ are, on average, 3° from the $[001]$ direction in rutile. However, there are six significant outliers, two that showed significant deviations in Fig. 5a and four others. The four new outliers have some characteristics in common. First, they are in the same region of orientation space, near the border between the anatase field and the rutile field (these are the points indicated by the solid squares in Fig. 3). Second, they have an approximately 30° misorientation from $[1\bar{1}0]$. Noting that

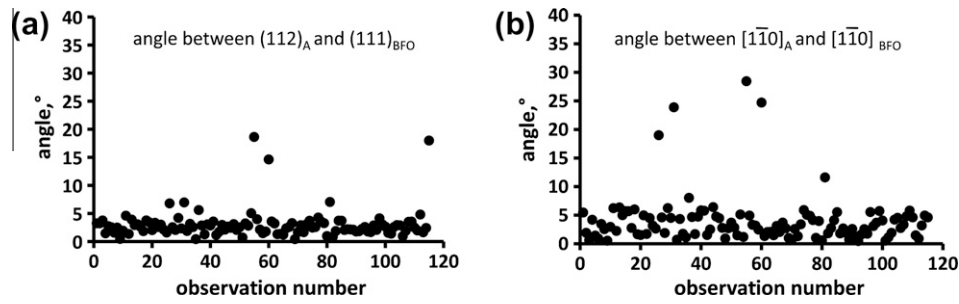


Fig. 4. Angles between low-index substrate and film orientations for 115 substrate/anatase pairs: (a) angle between $(111)_{\text{BFO}}$ and $(112)_{\text{A}}$; (b) angle between $[110]_{\text{A}}$ and $[1\bar{1}0]_{\text{BFO}}$.

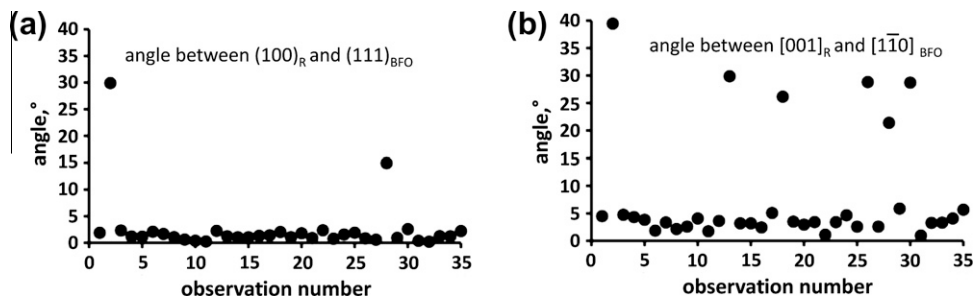


Fig. 5. Angles between low-index substrate and film orientations: (a) angle between $[111]_{\text{BFO}}$ and $[011]_{\text{R}}$; (b) angle between $[1\bar{1}0]_{\text{BFO}}$ and $[001]_{\text{R}}$.

the $[\bar{1}2\bar{1}]$ direction is also in the (111) plane and 30 from $[1\bar{1}0]$, the angles between $[\bar{1}2\bar{1}]$ and $[001]$ were calculated. For the four points in question, the average angle between $[\bar{1}2\bar{1}]$ and $[001]$ is 1.8° . From these observations, we conclude that there are two ORs. The dominant relationship representing 83% of the substrate/grain pairs is $(100)_{\text{R}} \parallel (111)_{\text{BFO}}$ and $[001]_{\text{R}} \parallel [1\bar{1}0]_{\text{BFO}}$.

As for the case of anatase, approximately 5% of the observations (two cases) are outliers. These points are marked by black triangles in Fig. 3. Calculations show that for these two cases, $(100)_{\text{R}} \parallel (210)_{\text{BFO}}$ are misaligned by an average of $6^\circ \pm 1^\circ$. However, as before, these minority observations were not considered further.

4. Discussion

The BiFeO_3 structure can be thought of a cubic close-packed (ccp) network of BiO_3 atoms, with Fe in one-quarter of the octahedral interstices. Anatase can be thought of as a ccp network of O with Ti in one-half of the octahedral interstices. Rutile can be thought of as a hexagonally close-packed (hcp) network of O with Ti in one half of the octahedral interstices. Considering these nearly closest-packed (eutactic) networks [34], the dominant observed ORs can be interpreted as having parallel closest-packed planes and closest-packed directions, as illustrated in Fig. 6a and b. For example, anatase can be thought of as two (distorted) ccp cells stacked along the $[001]$ direction. Therefore, the closest-packed planes of O atoms are (112) and this is the plane that is parallel to (111) in BiFeO_3 . The closest-packed directions in both of these planes is $[1\bar{1}0]$

and these directions are also aligned (see Fig. 4b). Rutile has its closest-packed layers in (100) planes that are stacked in an hcp sequence; these layers are parallel to the closest-packed (111) plane of the substrate. In this case, the ABC stacking of close-packed layers in BiFeO_3 changes to AB stacking of the layers in rutile. Therefore, the vast majority of the observed ORs can be described by saying that the closest-packed planes in the substrate and film are parallel and, within these planes, the closest-packed directions are parallel.

For the growth of anatase on perovskite substrates, the OR is usually reported as $(001)_{\text{A}} \parallel (001)_{\text{P}}$ and $[100]_{\text{A}} \parallel [100]_{\text{P}}$ for growth on (001) substrates [13–16,19,20,23,25–27] and $(012)_{\text{A}} \parallel (110)_{\text{P}}$ and $[100]_{\text{A}} \parallel [001]_{\text{P}}$ for growth on (110) substrates [17,20–22,24]. Although the indices of the planes for both ORs differ from one another and from our assignment, all three are essentially identical from a crystallographic perspective. In other words, when $(112)_{\text{A}} \parallel (111)_{\text{BFO}}$, this brings the (012) plane of anatase parallel to the (110) plane of perovskite. It also brings the two (001) planes into near-perfect alignment. To demonstrate that our data support all three descriptions, the angles between the $(012)_{\text{A}}$ and $(110)_{\text{BFO}}$ planes were calculated for the 115 substrate anatase pairs; the average misorientation (standard deviation) was $2.8^\circ (1.3^\circ)$. When the analysis is repeated for $(100)_{\text{A}}$ and $(100)_{\text{BFO}}$ the average misorientation (standard deviation) was $2.5^\circ (1.4^\circ)$, and for $(001)_{\text{A}}$ and $(001)_{\text{BFO}}$ the average misorientation (standard deviation) was $7.3^\circ (2.4^\circ)$. In other words, our experiments on high-index surfaces of BiFeO_3 are consistent with previous growth experiments on (001) and (110)

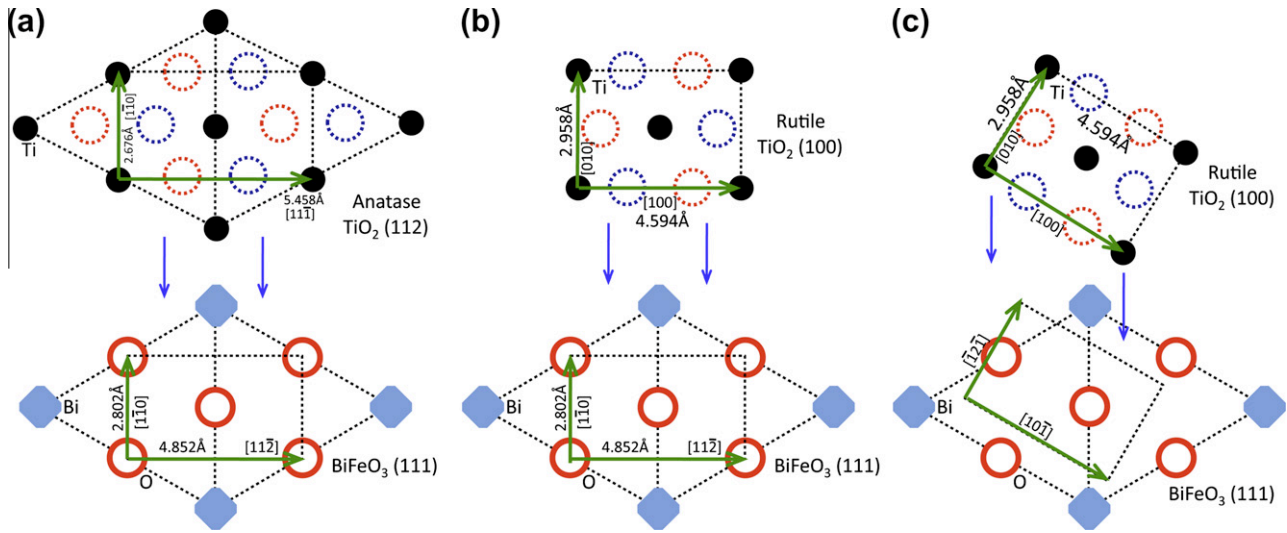


Fig. 6. Schematic depiction of the ORs between BiFeO₃ and TiO₂. In all drawings, light blue diamonds, red circles with complete lines, and black circles are Bi, O and Ti, respectively, in the plane of the drawing. The dashed blue circles are O in the closest-packed layer below the plane and the dashed red circles are O in the closest-packed layer above the plane. No attempt has been made to depict the unknown microscopic translations, although the Ti are expected to fill octahedral interstices and the O are expected to fill the closest packed positions. (a) (112)_A || (111)_{BFO} and $[1\bar{1}0]_A || [1\bar{1}0]_{BFO}$. (b) (100)_R || (111)_{BFO} and $[001]_R || [1\bar{1}0]_{BFO}$. (c) (100)_R || (111)_{BFO} and $[001]_R || [\bar{1}2\bar{1}]_{BFO}$. (For interpretation of the references to color in this figure legend, the reader is referred to the web version of this article.)

perovskite substrates. However, we argue that describing the OR as (112)_A || (111)_{BFO}, and $[1\bar{1}0]_A || [1\bar{1}0]_{BFO}$ is preferred because it emphasizes the continuity of the closest-packed networks.

For the growth of rutile on perovskite, the alignment of the closest-packed planes makes (100)_R parallel to (111)_{BFO} for 33 of 35 of the observed pairs. This is consistent with results reported for rutile grown on other perovskite structured compounds [13,21,22,27]. Two possible in-plane orientations have been identified here. In one case, the rutile *c*-axis, [001], is parallel to the $[1\bar{1}0]$ axis which aligns the closest-packed directions in the substrate and film. For this majority observation (83%), the epitaxy is again described as an alignment of the closest-packed planes and directions. For the minority (12%) OR, the [001] axis of rutile is parallel to the $[\bar{1}2\bar{1}]$ axis of BiFeO₃. These two arrangements are depicted schematically in Fig. 6b and c. The observation of two in-plane ORs indicates that they compete with one another during nucleation and the prevalence of the former indicates that a continuation of the close-packed arrangement is preferred. That they both still align closest-packed planes indicates that they are low-energy nucleation events. That the minority observation exists near the phase boundary of anatase and rutile indicates that the majority OR in rutile is less competitive in the nucleation process at these surface orientations. However, it should also be noted that the low number of observations makes it difficult to interpret at this time.

One puzzling aspect of the results presented here is that for BiFeO₃ substrate grains oriented within 10° of (111), the growth was polycrystalline and did not exhibit an obvious epitaxial relationship; considering that 94% of the

grains had an OR with (100)_R || (111)_{BFO}, one would expect epitaxial films with the same OR at the (111)_{BFO} orientation. In fact, it is well known that this OR is observed on other perovskite (111) single-crystal substrates [21,22,27]. The data available here do not suggest an explanation for this observation, and, in fact, this is not the goal of this paper. However, one might speculate that there is some instability in the BiFeO₃ (111) surface at the growth temperature that leads to poor growth. Selbach et al. [35] reported that when BiFeO₃ is heated at 600 °C for 30 min, the formation of Bi₂₉FeO₃₉ and Bi₂Fe₄O₉ can be detected in the X-ray diffraction patterns. The substrates in this study were annealed at this temperature to heal polishing damage before growth and this was also the nominal growth temperature. Therefore, it is possible that (111)-oriented surfaces decompose preferentially and this leads to surfaces unsuitable for epitaxial growth.

While the ORs that we identify are consistent with previous studies of titania epitaxy on perovskite, it is important to emphasize the vast majority of the observed substrate/film pairs did not share the low-index interface planes characteristic of the previous work. One might argue that even though high-index surfaces are used as substrates, they could be microfaceted and that growth actually nucleates on low-index terraces and then spreads across the entire grain surface. To test this idea, the substrate surfaces were imaged by atomic force microscopy (AFM). However, because no clear facets were observed, the results were inconclusive (the negative observation does not rule out the possibility of nanostructured facets beyond the resolution of the AFM). The best evidence for the existence of terraces is illustrated in Fig. 7, which provides some indication of orientated ledges. However, in no case

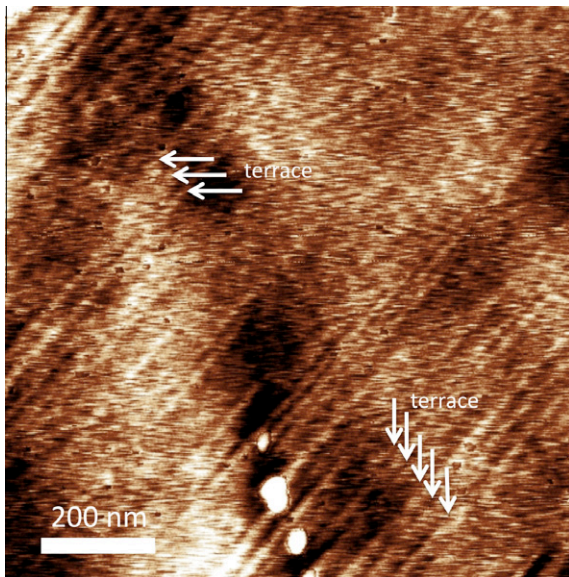


Fig. 7. AFM image of a BiFeO₃ grain misoriented $\sim 10^\circ$ from (100)_{BFO}. Some of the contrast suggests the presence of terraces (see white arrows). The contrast from bright to dark is 2 nm.

were distinct facets observed and the largest structured features that we detected were less than 2 nm in height and approximately 20 nm in lateral extent. Therefore, the evidence that the high-index surfaces facet to low-index orientations is weak.

The conclusion that the underlying principle governing the ORs in the BiFeO₃/TiO₂ system is the alignment of closest-packed planes and directions was made possible by examining ORs on a wide range of high-index surfaces, using a new method we refer to as CSE. Compared to film growth experiments on single-crystal substrates, the CSE technique allows hundreds of film growth experiments to be conducted in parallel and can, therefore, be considered a high-throughput method for investigating ORs. In addition to the highly parallel nature of the technique, there are other advantages. For example, by using polycrystalline substrates, it is possible to grow on phases that cannot be obtained in single-crystal form. Using polycrystalline substrates, it is also relatively easy to alter the lattice parameter by forming a solid solution. Finally, by conducting many growth experiments at once, competitive ORs can be detected and, if of interest, might be stabilized by adjusting the temperature or the lattice parameters of the substrate through alloying.

5. Conclusion

A new technique for the high-throughput study of ORs, called CSE, has been demonstrated on the BiFeO₃/TiO₂ system. Titania films deposited on BiFeO₃ at 600 °C using PLD are epitaxial for all substrate orientations more than 10° from (111). Anatase films grow on BiFeO₃ substrates with an epitaxial relationship of (112)_A|| (111)_{BFO}, and

$[1\bar{1}0]_A || [1\bar{1}0]_{BFO}$; rutile TiO₂ films grow on BiFeO₃ substrates with (100)_R|| (111)_{BFO} and $[001]_R || [1\bar{1}0]_{BFO}$ or (100)_R|| (111)_{BFO} and $[001]_R || [\bar{1}2\bar{1}]_{BFO}$. Anatase grows on substrate orientations within about 35° of (001) and rutile films grow on orientations further away. The persistence of strong epitaxy on the highest-index surfaces suggests that the three-dimensional alignment of the closest-packed networks is important and that lattice matching in specific low-index planes is a special case of this more general phenomenon. The dominant ORs align the closest-packed directions and planes of the substrate and film.

Acknowledgement

The work was supported by National Science foundation Grants DMR 0804770 and DMR 1206656.

Appendix A. Supplementary material

Supplementary data associated with this article can be found, in the online version, at <http://dx.doi.org/10.1016/j.actamat.2012.07.060>.

References

- [1] Burbure NV, Salvador PA, Rohrer GS. *J Am Ceram Soc* 2006;89:2943.
- [2] Burbure NV, Salvador PA, Rohrer GS. *Chem Mater* 2010;22:5831.
- [3] Burbure NV, Salvador PA, Rohrer GS. *Chem Mater* 2010;22:5823.
- [4] Zhang YL, Schultz AM, Salvador PA, Rohrer GS. *J Mater Chem* 2011;21:4168.
- [5] Fox MA, Dulay MT. *Chem Rev* 1993;93:341.
- [6] Hengerer R, Kavan L, Krtil P, Grätzel M. *J Electrochem Soc* 2000;147:1467.
- [7] Hotsenpiller PAM, Bolt JD, Farneth WE, Lowekamp JB, Rohrer GS. *J Phys Chem B* 1998;102:3216.
- [8] Lowekamp JB, Rohrer GS, Hotsenpiller PAM, Bolt JD, Farneth WE. *J Phys Chem B* 1998;102:7323.
- [9] Gorbenko OY, Samoilenkov SV, Graboy IE, Kaul AR. *Chem Mater* 2002;14:4026.
- [10] Moreau JM, Michel C, Gerson R, James WJ. *J Phys Chem Solids* 1971;32:1315.
- [11] Geller S, Bala VB. *Acta Crystallogr* 1956;9:1019.
- [12] Okazaki A, Kawamina M. *Mater Res Bull* 1973;8:545.
- [13] Burbure NV, Salvador PA, Rohrer GS. *J Am Ceram Soc* 2010;93:2530.
- [14] Chambers SA, Wang CM, Thevuthasan S, Droubay T, McCready DE, Lea AS, et al. *Thin Solid Films* 2002;418:197.
- [15] Chen S, Mason MG, Gysling HJ, Pazpujalt GR, Blanton TN, Castro T, et al. *J Vac Sci Technol A – Vac Surf Films* 1993;11:2419.
- [16] Fisher P, Maksimov O, Du H, Heydemann VD, Skowronski M, Salvador PA. *Microelectron J* 2006;37:1493.
- [17] Gao W, Klie R, Altman EI. *Thin Solid Films* 2005;485:115.
- [18] Herman GS, Gao Y. *Thin Solid Films* 2001;397:157.
- [19] Hsieh CC, Wu KH, Juang JY, Uen TM, Lin JY, Gou YS. *J Appl Phys* 2002;92:2518.
- [20] Kennedy RJ, Stampe PA. *J Cryst Growth* 2003;252:333.
- [21] Lotnyk A, Senz S, Hesse D. *Thin Solid Films* 2007;515:3439.
- [22] Lotnyk A, Senz S, Hesse D. *J Phys Chem C* 2007;111:6372.
- [23] Murakami M, Matsumoto Y, Nakajima K, Makino T, Segawa Y, Chikyow T, et al. *Appl Phys Lett* 2001;78:2664.
- [24] Silva VF, Bouquet V, Deputier S, Boursicot S, Ollivier S, Weber IT, et al. *J Appl Crystallogr* 2010;43:1502.

- [25] Sugimura W, Yamazaki T, Shigetani H, Tanaka J, Mitsuhashi T. *Jpn J Appl Phys Part 1 – Reg Pap Short Notes Rev Pap* 1997;36:7358.
- [26] Weng X, Fisher P, Skowronski M, Salvador PA, Maksimov O. *J Cryst Growth* 2008;310:545.
- [27] Yamamoto S, Sumita T, Yamaki T, Miyashita A, Naramoto H. *J Cryst Growth* 2002;237:569.
- [28] Howard CJ, Sabine TM, Dickson F. *Acta Crystallogr Sec B – Struct Sci* 1991;47:462.
- [29] Rhodes RG. *Acta Crystallogr* 1951;4:105.
- [30] Schultz AM, Zhang YL, Salvador PA, Rohrer GS. *ACS Appl Mater Interf.* 2011;3:1562.
- [31] Adams BL, Wright SI, Kunze K. *Metal Trans A* 1993;24:819.
- [32] Lowndes DH, Geohegan DB, Poretzky AA, Norton DP, Rouleau CM. *Science* 1996;273:898.
- [33] Humphreys FJ, Huang Y, Brough I, Harris C. *J Microsc* 1999;195:212.
- [34] Okeeffe M. *Acta Crystallogr Sec A* 1977;33:924.
- [35] Selbach SM, Einarsrud MA, Grande T. *Chem Mater* 2009;21:169.